

## PAPER

# Pixel-Level Color Demodulation Image Sensor for Support of Image Recognition

Yusuke OIKE<sup>†a)</sup>, Student Member, Makoto IKEDA<sup>†</sup>, and Kunihiro ASADA<sup>†</sup>, Members

**SUMMARY** In this paper, we present a pixel-level color image sensor with efficient ambient light suppression using a modulated RGB flashlight to support a recognition system. The image sensor employs bidirectional photocurrent integrators for pixel-level demodulation and ambient light suppression. It demodulates a projected flashlight with suppression of an ambient light at short intervals during an exposure period. In the imaging system using an RGB modulated flashlight, every pixel provides innate color and depth information of a target object for color-based categorization and depth-key object extraction. We have designed and fabricated a prototype chip with  $64 \times 64$  pixels using a  $0.35 \mu\text{m}$  CMOS process. Color image reconstruction and time-of-flight range finding have been performed for the feasibility test.

**key words:** image sensor, pixel-level color imaging, modulated RGB flashlight, object extraction, time-of-flight range finding, image recognition

## 1. Introduction

In recent years, image recognition systems have become important in applications such as security systems, intelligent transportation systems (ITS), factory automation, and robotics. Object extraction from a captured scene is important for such recognition systems. Object extraction generally requires huge computational effort, thus, it is desirable to extract target objects by flashlight decay [1] or time-of-flight (TOF) range finding [2], as shown in Fig. 1. Color information is also useful for identifying a target object. However, it is difficult for a standard image sensor to acquire the innate color since the color imaging results are strongly affected by ambient illumination. Therefore, a function of ambient light suppression is efficient for image recognition.

Some image sensors with photocurrent demodulation have been presented for suppressing a constant light [3]–[6]. The conventional techniques [3], [4] involve the use of two photocurrent integrators. One accumulates a signal light and an ambient light together, and then the other accumulates only an ambient light. Therefore, its dynamic range is limited by the ambient light intensity. A logarithmic-response position sensor [5], [6] expands the dynamic range through adaptive ambient light suppression. The signal gain, however, changes with the incident light intensity, hence it is not suitable for imaging a scene. We have proposed an imaging system configuration using a modulated flashlight and a demodulation image sensor for support of image recognition in various measurement situations [7]. It is capable

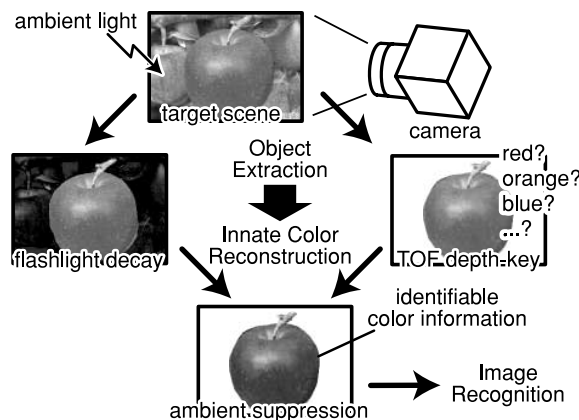


Fig. 1 Preprocessing for image recognition.

of providing innate color and depth information of a target object for color-based categorization and depth-key object extraction.

In this paper, we present a pixel-level color image sensor with efficient ambient light suppression using a modulated RGB flashlight. The image sensor employs bidirectional photocurrent integrators for pixel-level demodulation and ambient light suppression. It demodulates a projected flashlight with suppression of an ambient light at short intervals during an exposure period. The demodulation function contributes to avoid saturation from ambient illumination. Every pixel provides innate color information without false color or intensity loss of color filters. The demodulation function is capable of TOF range finding to realize depth-key object extraction. We have designed and fabricated a prototype chip with  $64 \times 64$  pixels using a  $0.35 \mu\text{m}$  CMOS process.

In Sect. 2, the imaging system configuration using a modulated RGB flashlight is described. The proposed sensing scheme with efficient ambient light suppression is presented and compared with the conventional one in Sect. 3. In Sect. 4, we illustrate the pixel circuit configuration and operation. Section 5 is on the sensor block diagram and chip implementation. The measurement results and performance comparison are discussed in Sect. 6, and conclusions are given in Sect. 7.

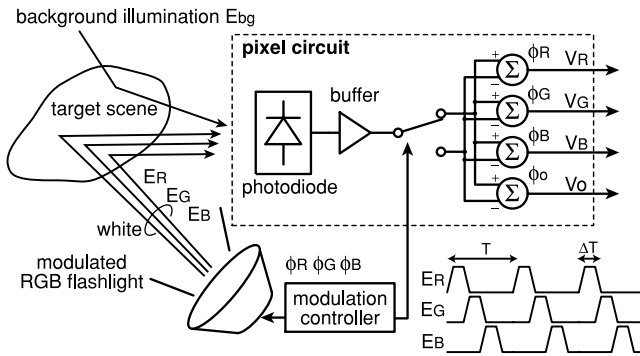
## 2. System Configuration

Figure 2 shows an imaging system configuration with a

Manuscript received June 9, 2004.

<sup>†</sup>The authors are with the Faculty of Engineering, and VLSI Design and Education Center (VDEC), the University of Tokyo, Tokyo, 113-8656 Japan.

a) E-mail: y-oike@silicon.u-tokyo.ac.jp



**Fig. 2** System configuration with a modulated RGB flashlight.

modulated RGB flashlight. The RGB flashlight contains three color projections, which are modulated by  $\phi_R$ ,  $\phi_G$ , and  $\phi_B$ , respectively. The duty ratio is set to 25%. Each modulation phase is shifted 90 degrees. A photodetector receives the modulated light,  $E_R$ ,  $E_G$ , and  $E_B$ , from a target scene together with an ambient light,  $E_{bg}$ . An ambient light is provided from the sun, a fluorescent light, etc. Therefore, the ambient light intensity,  $E_{bg}$ , is constant or low frequent. A photocurrent,  $I_{pd}$ , is generated in proportion to the incident intensity,  $E_{total}$ , as follows:

$$I_{pd} \propto E_{total} = \begin{cases} E_R + E_{bg}, & \text{if } t = nT \sim nT + \Delta T \\ E_G + E_{bg}, & \text{if } t = nT + \Delta T \sim nT + 2\Delta T \\ E_B + E_{bg}, & \text{if } t = nT + 2\Delta T \sim nT + 3\Delta T \\ E_{bg}, & \text{otherwise,} \end{cases} \quad (1)$$

where  $T$  is the cycle time of modulation,  $\Delta T$  is the pulse width of each flashlight, and  $n$  is the number of modulation cycles during exposure. The photodetector has four integrators with a demodulation function.  $I_{pd}$  is accumulated in each integrator synchronized with  $\phi_R$ ,  $\phi_G$ , and  $\phi_B$ . Then, in all integrators, the ambient light level,  $E_{bg}$ , is subtracted from the total level in one modulation cycle of  $T$ . The short-interval subtraction contributes to the suppression of the influence of an ambient light on color information. The color sensing incurs no intensity loss caused by color filters.

Flashlight imaging originally realizes rough range finding based on flashlight decay [1] although it is sometimes utilized for object extraction the reliability is influenced by surface reflectance. Thus, it is difficult to identify multiple objects in a target scene. On the other hand, TOF range finding attains more efficient object extraction, which is called a depth-key technique [2]. A demodulation function is capable of TOF range finding as presented in [8], [9], and the present system is also capable of depth-key object extraction.

### 3. Sensing Scheme with Ambient Light Suppression

Conventional demodulation sensors [3], [4] have two photocurrent integrators as shown in Fig. 3(a). Photocurrents,  $I_{sig}$  and  $I_{bg}$ , are generated by a modulated light,  $E_{sig}$ , and an

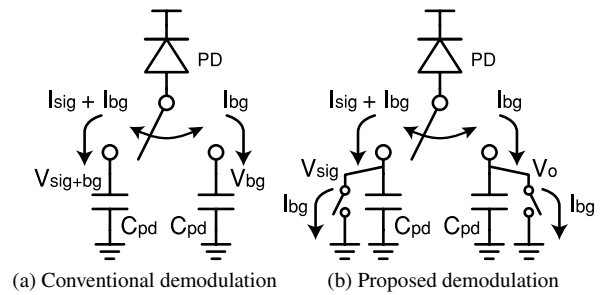


**Fig. 3** Photocurrent demodulation by two in-pixel integrators.

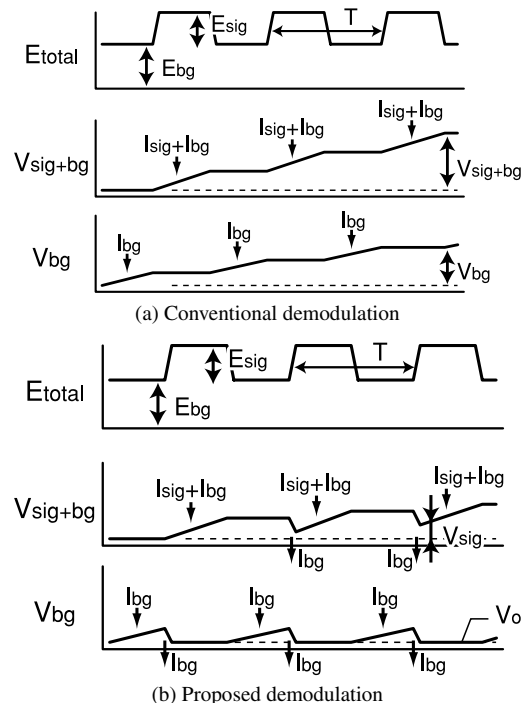


**Fig. 4** Timing diagram of photocurrent demodulation.

ambient light,  $E_{bg}$ , respectively. While the flashlight projection is turned on, the total photocurrent of  $I_{sig}$  and  $I_{bg}$  is accumulated in one of the photocurrent integrators as shown in Fig. 4(a). And then,  $I_{bg}$  is accumulated in the other photocurrent integrator while the flashlight projection is turned off. The signal level,  $V_{sig}$ , is calculated from the accumulation results,  $V_{sig+bg}$  and  $V_{bg}$ , after the exposure period.

$$\begin{aligned} V_{sig} &= V_{sig+bg} - V_{bg} \\ &= \sum_{i=0}^n \frac{(I_{sig} + I_{bg}) \cdot \Delta T}{C_{pd}} - \sum_{i=0}^n \frac{I_{bg} \cdot \Delta T}{C_{pd}}, \end{aligned} \quad (2)$$

where  $C_{pd}$  is the parasitic capacitance of a photodiode. Therefore, the dynamic range of conventional demodulation sensors is limited by the saturation level  $V_{sat}$  as follows:

$$V_{sig+bg} < V_{sat}. \quad (3)$$

In the conventional techniques, the signal level easily saturates owing to an ambient light.

On the other hand, the present sensing scheme suppresses an ambient light at short intervals during the exposure period as shown in Fig. 3(b) and Fig. 4(b). In a modulation cycle, the photocurrents,  $I_{sig}$  and  $I_{bg}$ , are accumulated in each photocurrent integrator in the same way as in the conventional sensing scheme. Then, the ambient light intensity is subtracted from the output of photocurrent integrators in every modulation cycle. Therefore, the signal level  $V_{sig}$  is directly provided by the pixel output as follows:

$$V_{sig} = \sum_{i=0}^n \left( \frac{(I_{sig} + I_{bg}) \cdot \Delta T}{C_{pd}} - \frac{I_{bg} \cdot \Delta T}{C_{pd}} \right). \quad (4)$$

Thus, the dynamic range is given by

$$V_{sig} < V_{sat}. \quad (5)$$

In the present sensing scheme, a short demodulation cycle of  $T$  makes the dynamic range higher since it avoids the saturation caused by an ambient light. The other photocurrent integrator provides  $V_O$  as the offset level to cancel the asymmetry of bidirectional integration.

### 4. Pixel Circuit Configuration and Operation

#### 4.1 Pixel-Level Color Demodulation

The present sensing scheme employs a bidirectional photocurrent integrator. It is implemented through the use of discrete-time voltage integrators and a fully differential amplifier with bidirectional output drive as shown in Fig. 5(a). The gain of the fully differential amplifier is set to 1. In this implementation, the photodetector has two integrators. Thus, a full-color pixel requires three photodetectors, which comprise three photodiodes, three amplifiers, and six photocurrent integrators in total. In the present imaging system, a photodiode can be shared by the integrators as shown in Fig. 5(b), since three color projections are separately modulated as shown in Fig. 5(c). The pixel-level color demodulation reduces the circuit area required for full-color imaging.

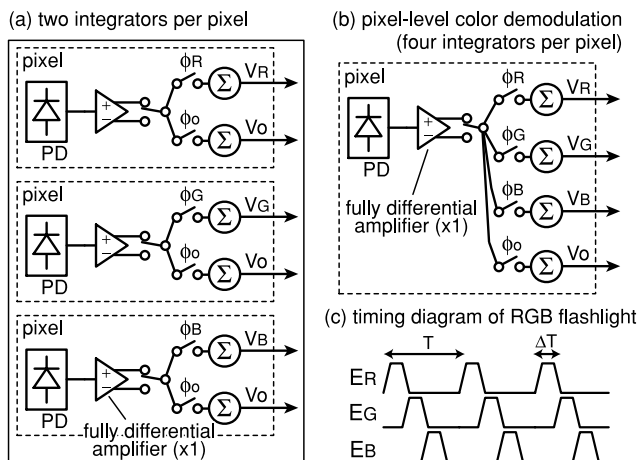


Fig. 5 Pixel configuration.

Furthermore, a captured color image has no false color due to the pixel-level imaging.

#### 4.2 Circuit Configuration

Figure 6 shows a pixel circuit configuration and a pixel layout in a 0.35 μm CMOS process technology. It consists of a photodiode (PD), a fully differential amplifier, four integrators ( $\Sigma_i$ ) with a demodulation function, and four source follower circuits. The gain of the fully differential amplifier is set to 1. The pixel size is 33.0 μm × 33.0 μm with a 12.4% fill factor.

Figure 7 shows a timing diagram of the pixel circuit.  $\phi_{rst}$  initializes all photocurrent integrators.  $\phi_{pd}$  resets  $V_{pd}$  at a photodiode.  $\phi_p$  and  $\phi_m$  switch between an accumulation mode and a subtraction mode.  $\phi_s$  and  $\phi_h$  perform a sample-and-hold operation for four integrators.  $\phi_r$ ,  $\phi_g$ ,  $\phi_b$ , and  $\phi_o$  activate a photocurrent integrator. In the reset period, all in-

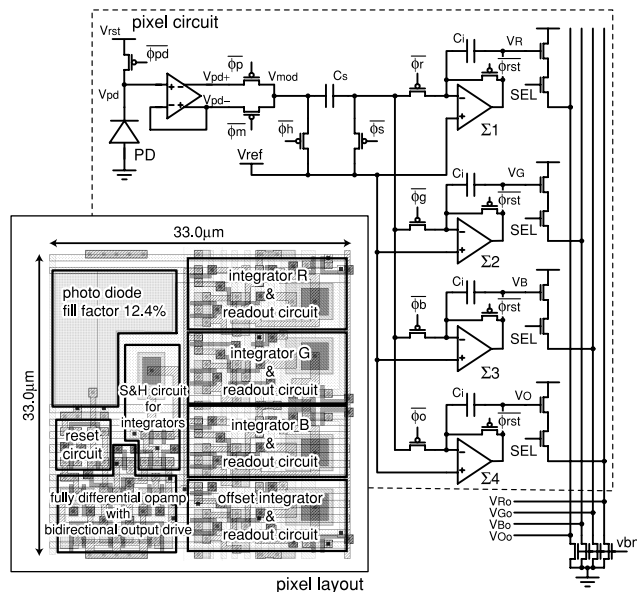


Fig. 6 Pixel circuit configuration and layout in a 0.35 μm process technology.

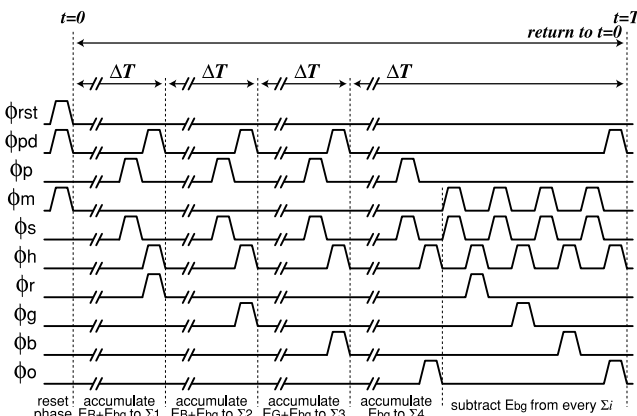


Fig. 7 Timing diagram.

tegrators are initialized by  $\phi_{rst}$ , and  $V_{pd}$  at the photodiode is reset to  $V_{rst}$  by  $\phi_{pd}$ . In the first  $\Delta T$ , the photodetector accumulates the total photocurrent of  $I_R$  and  $I_{bg}$  in a photocurrent integrator,  $\Sigma_1$ , since a projected flashlight contains a red light of  $E_R$ . Then, it accumulates  $I_G$  and  $I_B$  together with  $I_{bg}$  in  $\Sigma_2$  and  $\Sigma_3$  in the second and third  $\Delta T$ , respectively, after  $V_{pd}$  is reset again. Finally,  $I_{bg}$  is accumulated in  $\Sigma_4$ , and subtracted from all integrators in the fourth  $\Delta T$ . The modulation cycle,  $T$ , is repeated during the exposure period. The pixel values,  $V_R$ ,  $V_G$ ,  $V_B$ , and  $V_O$ , are read out through the source follower circuits as output signals,  $V_{Ro}$ ,  $V_{Go}$ ,  $V_{Bo}$ , and  $V_{Oo}$ .

### 4.3 Asymmetry Offset of Bidirectional Integration

The discrete-time voltage integrator,  $\Sigma_i$ , accumulates a voltage level of  $V_{mod}$ . The input voltage of  $\Sigma_i$  is given by

$$V_{mod} = \begin{cases} V_{pd+}, & \text{if } \phi_p = H \text{ and } \phi_m = L \\ V_{pd-}, & \text{if } \phi_p = L \text{ and } \phi_m = H. \end{cases} \quad (6)$$

The bidirectional integration is realized by switching two outputs of the fully differential amplifier,  $V_{pd+}$  and  $V_{pd-}$ , as shown in Fig. 8. They are given by

$$V_{pd+} = A_p \cdot \Delta V_{pd} - \Delta V_+, \quad (7)$$

$$V_{pd-} = -(A_m \cdot \Delta V_{pd} - \Delta V_-), \quad (8)$$

$$\Delta V_{pd} = \frac{I_{total} \cdot \Delta T}{C_{pd}}, \quad (9)$$

$$A_p \approx A_m \approx 1, \quad (10)$$

where  $A_p$  and  $A_m$  are the gain of the fully differential amplifier in the accumulation mode and the subtraction mode, respectively. Both are set to 1, but they are not exactly the same because of the device fluctuation.  $\Delta V_+$  and  $\Delta V_-$  are the offset levels of  $V_{pd+}$  and  $V_{pd-}$  from the reference voltage  $V_{ref}$ , respectively.  $I_{total}$  is the photocurrent generated by an incident light. From Eq. (4), we have

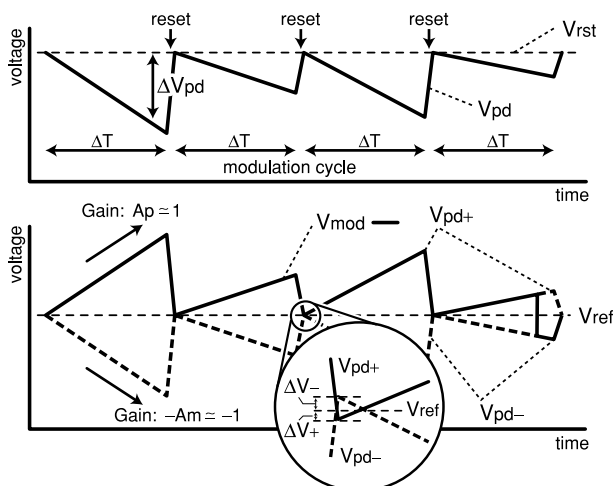


Fig. 8 Asymmetry offset of bidirectional integration.

$$V_{sig} = \sum_{i=0}^n \left( (A_p \cdot \Delta V_{sig+bg} - \Delta V_+) - (A_m \cdot \Delta V_{bg} - \Delta V_-) \right), \quad (11)$$

considering the offset variations of bidirectional integration.  $\Delta V_{sig+bg}$  and  $\Delta V_{bg}$  are given by

$$\Delta V_{sig+bg} = \frac{(I_{sig} + I_{bg}) \cdot \Delta T}{C_{pd}}, \quad (12)$$

$$\Delta V_{bg} = \frac{I_{bg} \cdot \Delta T}{C_{pd}}. \quad (13)$$

Substituting Eq. (12) and Eq. (13) into Eq. (11) gives

$$V_{sig} = V_{out} + \Delta V_{gain} + \Delta V_{bias}. \quad (14)$$

$V_{out}$  is the signal level required for a color image.  $\Delta V_{gain}$  is the offset level caused by the gain variations.  $\Delta V_{bias}$  is the offset level caused by the bias fluctuations.

$$V_{out} = \frac{A_p \cdot I_{sig} \cdot n \Delta T}{C_{pd}}, \quad (15)$$

$$\Delta V_{gain} = \frac{(A_p - A_m) \cdot I_{bg} \cdot n \Delta T}{C_{pd}}, \quad (16)$$

$$\Delta V_{bias} = -n(\Delta V_+ - \Delta V_-). \quad (17)$$

On the other hand, the fourth integrator accumulates  $I_{bg}$ , and then it subtracts  $I_{bg}$  from the accumulation. The output level,  $V_O$ , is given by

$$\begin{aligned} V_O &= \sum_{i=0}^n \left( (A_p \cdot \Delta V_{bg} - \Delta V_+) - (A_m \cdot \Delta V_{bg} - \Delta V_-) \right) \\ &= \Delta V_{gain} + \Delta V_{bias}. \end{aligned} \quad (18)$$

Therefore, the significant signal level  $V_{out}$  is acquired as follows.

$$V_{out} = V_{sig} - V_O. \quad (19)$$

The fourth integrator contributes to the suppression of the asymmetry offset of bidirectional integration.

### 4.4 Simulation of Pixel-Level Demodulation

Figure 9 shows simulation waveforms of pixel-level demodulation with efficient ambient light suppression. Under the simulation conditions, a photocurrent,  $I_{bg}$ , is set to 200 nA, which is generated by an ambient light of  $E_{bg}$ . Signal photocurrents,  $I_R$ ,  $I_G$ , and  $I_B$ , are set to 40 nA, 80 nA, and 120 nA, respectively, which are generated by a modulated RGB flashlight. The parasitic capacitance of a photodiode,  $C_{pd}$ , is 73 fF. The sampling capacitance,  $C_s$ , is 12 fF. The integration capacitance,  $C_i$ , is 17 fF.  $\Delta T$  is set to 0.1 ms. A modulation cycle of 0.4 ms is repeated 25 times during the exposure time.

The signal levels are acquired to be  $|V_R - V_O|$ ,  $|V_G - V_O|$ , and  $|V_B - V_O|$  with the suppression of an ambient light  $E_{bg}$  as shown by (a)–(c) in Fig. 9.  $V_O$  is the output of the fourth

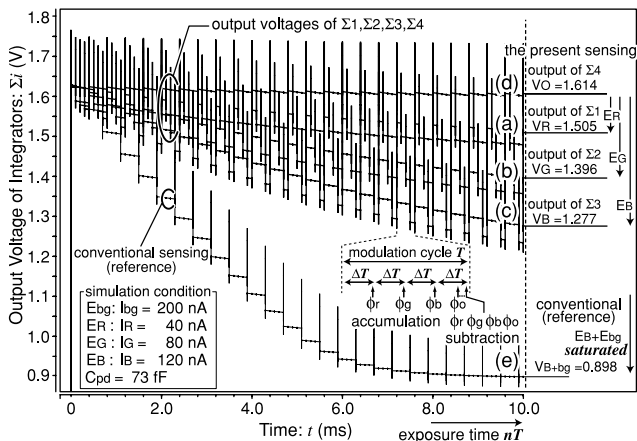


Fig. 9 Simulation waveforms of pixel-level demodulation: (a)–(d) present sensing scheme, (e) conventional sensing scheme.

integrator, and it indicates the asymmetry offset of bidirectional integration as shown by Eq. (18). The present sensing scheme avoids saturation from ambient light intensity,  $E_{bg}$ , as shown by Eq. (4). In conventional sensing as shown by (e) in Fig. 9, the signal level can be saturated by a strong ambient light intensity since the integrator accumulates  $E_B$  and  $E_{bg}$  together without suppressing  $E_{bg}$  during the exposure period as described by Eq. (2).

5. Chip Implementation

We have designed and fabricated a prototype image sensor with  $64 \times 64$  pixels in a  $0.35 \mu\text{m}$  CMOS process. Figure 10 illustrates the sensor block diagram. The sensor consists of a  $64 \times 64$  pixel array, a row select decoder, control signal drivers, column amplifiers with a column select decoder, a correlation double sampling (CDS) circuit, an offset canceller, an 8-bit charge-distributed ADC, and a sensor controller. The CDS circuit suppresses the fixed-pattern noise caused by the column amplifiers. The offset canceller, which is shown in Fig. 11, subtracts the demodulation offset level,  $V_{Oo}$ , from signal output voltages,  $V_{Ro}$ ,  $V_{Go}$ , and  $V_{Bo}$ . The signal output voltages are sampled by  $\phi_{sub}$  at capacitors,  $C_{sub}$ , and then  $V_{Oo}$  is subtracted from them.  $V_{zero}$  is a bias level of the CDS circuit. All components are operated by an on-chip sensor controller. Figure 12 shows the chip microphotograph. Specifications of the prototype image sensor are summarized in Table 1.

6. Measurement Results

6.1 Efficient Ambient Light Suppression

Figure 13 shows measurement results of a signal output voltage,  $|V_{Ro} - V_{Oo}|$ , as a function of a modulated light intensity,  $E_R$ . A modulated light and a constant light are directly projected onto the sensor plane using red LEDs of 630 nm wavelength. The modulated light has a modulation cycle of 0.2 ms and a pulse width of 0.05 ms. The exposure time is

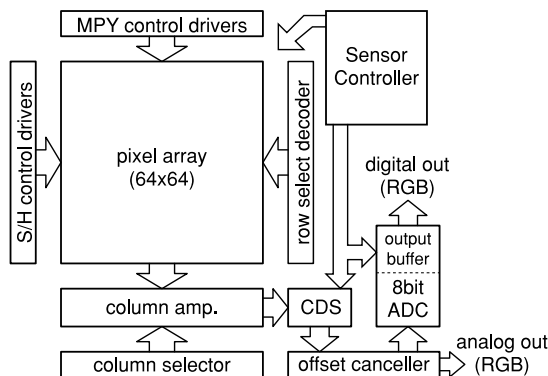


Fig. 10 Sensor block diagram.

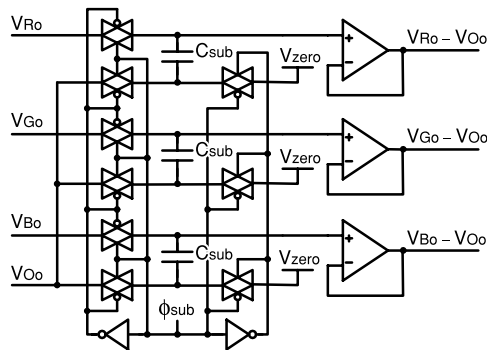


Fig. 11 Schematic of offset canceller.

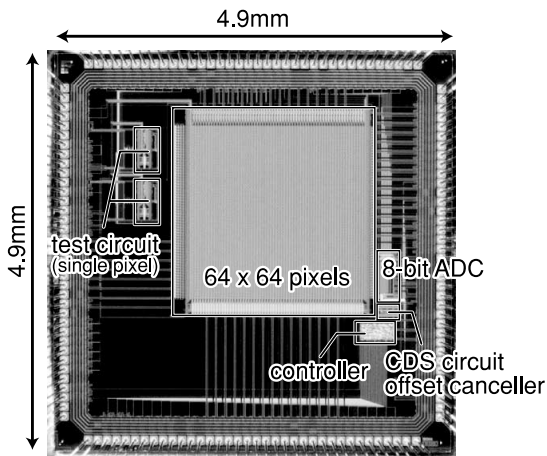
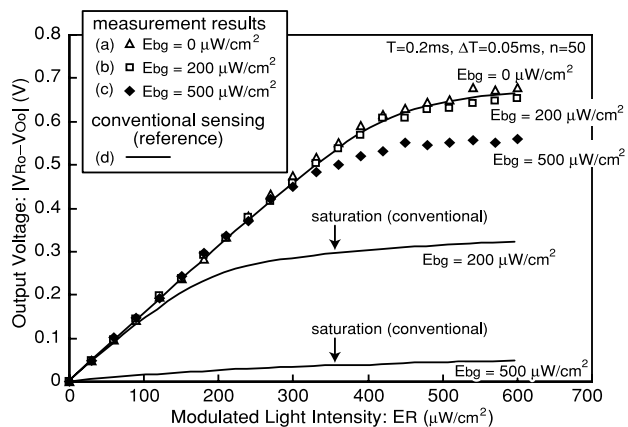


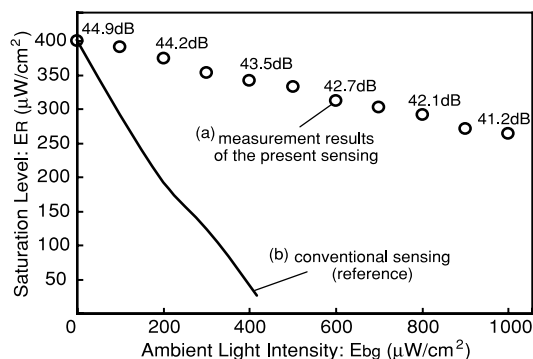
Fig. 12 Chip microphotograph.

Table 1 Specifications of the prototype image sensor.

Process	3-metal 2-poly-Si $0.35 \mu\text{m}$ CMOS
Die size	$4.9 \text{ mm} \times 4.9 \text{ mm}$
# of pixels	$64 \times 64$ pixels
Pixel size	$33.0 \mu\text{m} \times 33.0 \mu\text{m}$
Pixel config.	1 PD, 57 FETs and 5 capacitors
Fill factor	12.4%



**Fig. 13** Output voltage vs. modulated light intensity  $E_R$ : (a)  $E_{bg} = 0 \mu\text{W}/\text{cm}^2$ , (b)  $E_{bg} = 200 \mu\text{W}/\text{cm}^2$ , (c)  $E_{bg} = 500 \mu\text{W}/\text{cm}^2$ , (d) conventional demodulation without efficient ambient light suppression.



**Fig. 14** Saturation level of  $E_R$  vs. ambient light intensity  $E_{bg}$ : (a) measurement results of present sensing scheme, (b) reference of conventional sensing scheme.

10 ms. Figure 13(a) shows a signal output voltage with no ambient light. In this case, the present demodulation technique has high linearity as in the conventional demodulation technique. On the other hand, Fig. 13(d) shows that the conventional technique saturates the signal level because of the strong ambient light of  $200 \mu\text{W}/\text{cm}^2$  and  $500 \mu\text{W}/\text{cm}^2$ . In these cases, the present demodulation technique efficiently avoids saturation and maintains high linearity as shown by (b) and (c) in Fig. 13. The noise floor of the prototype image sensor is  $15.6 \text{ mV}_{\text{p-p}}$  and  $3.4 \text{ mV}_{\text{rms}}$ , which is measured as  $|V_{Ro} - V_{Oo}|$  under a constant light. It includes the gain variations caused by integration capacitance fluctuations of  $C_i$ .

Figure 14 shows the saturation level of a modulated light intensity,  $E_R$ , as a function of an ambient light intensity,  $E_{bg}$ . Figure 14(b) shows that the conventional technique is not suitable for various ambient light conditions since the saturation level is limited by the total level of  $E_R$  and  $E_{bg}$ . On the other hand, the saturation level of the present technique is not limited by the total intensity as shown in Fig. 14(a) though it is slightly affected by an offset level,  $V_{Oo}$ , caused by the asymmetry of bidirectional integration. Therefore, the present image sensor is capable of various

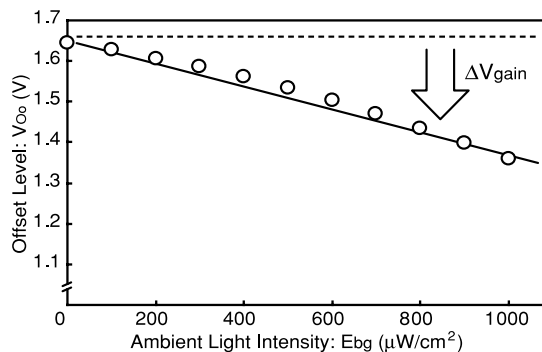


**Fig. 15** Offset voltage  $V_{Oo}$  vs. ambient light intensity  $E_{bg}$ .

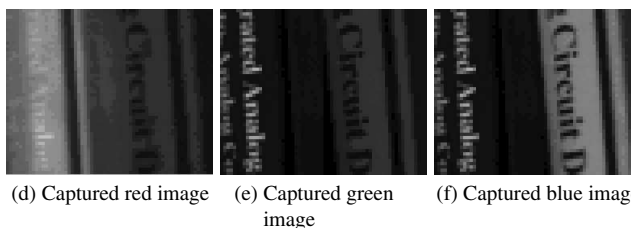
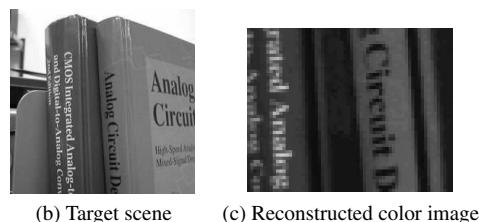
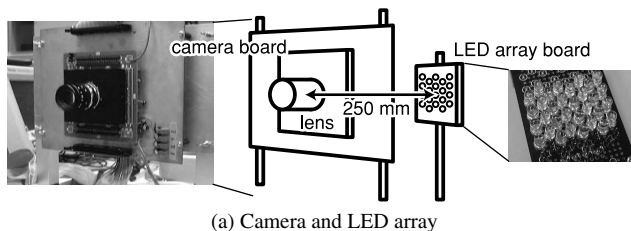


**Fig. 16** Measurement results of color imaging with ambient light suppression.

measurement situations.

Figure 15 shows the reason why the saturation level decreases with increasing an ambient light intensity in the present demodulation technique. Ideally, the offset level,  $V_{Oo}$ , is independent of  $E_{bg}$ . However, it contains an offset factor caused by the gain variation,  $\Delta V_{gain}$ , as shown by Eq. 16.  $\Delta V_{gain}$  is proportional to an ambient light intensity. Thus, the saturation level of  $V_{sig}$  in Eq. 14 decreases because of the asymmetric offset of bidirectional integration.

## 6.2 Pixel-Level Color Imaging

We have demonstrated color imaging using the present image sensor and a modulated RGB flashlight as shown in Fig. 16. The prototype flashlight projector has 8 red LEDs, 8 green LEDs and 16 blue LEDs, whose wavelengths are 630 nm, 520 nm and 470 nm, respectively. It is placed at a

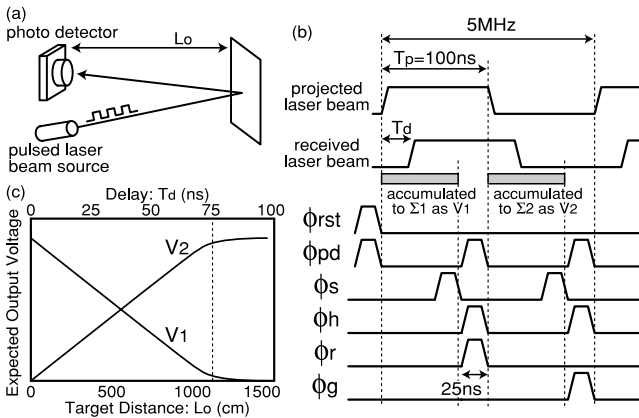


**Fig. 17** Timing diagram and expected output voltage of time-of-flight range finding.

distance of 250 mm alongside the camera board as shown in Fig. 16(a). The total power consumption of the flashlight projector is 474 mW. The flashlight and an ambient light of a fluorescent lamp provide around 500 lux and 120 lux of illumination, respectively, on a target scene at a distance of 300 mm from the sensor. Color image reconstruction requires the modulated flashlight intensity, the flashlight distribution on the target scene, and the spectral-response characteristics of the image sensor. In this measurement, we acquired the sensitivity of all pixels for the prototype flashlight projector by using a white board. It provides calibration parameters for nonuniformity of a modulated flashlight, spectral-response characteristics and sensitivity variations from integration capacitance fluctuations. The target scene is shown in Fig. 16(b), and the captured color image is shown in Fig. 16(c). It is reconstructed from the sensor outputs in Figs. 16(d)–(f). It contains color information corresponding to  $64 \times 64 \times 3$  pixels of a standard color imager since every pixel provides RGB colors.

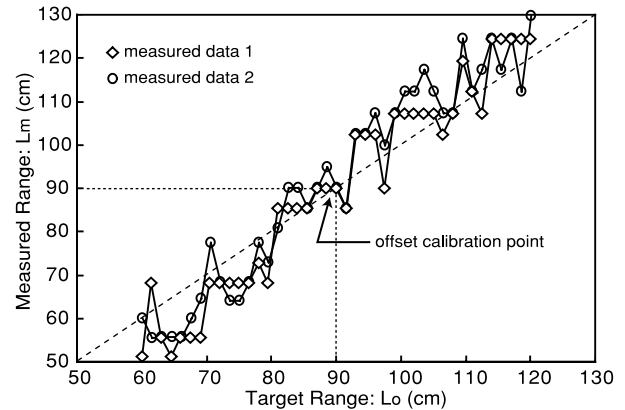
### 6.3 Time-of-Flight Range Finding

Figure 17(a) shows the system configuration of TOF range finding. A pulsed light is reflected from a target object with a delay time of  $T_d$  as shown in Fig. 17(b). The delay,  $T_d$ , as a result of the target distance,  $L_o$ , changes the demodulation outputs,  $V_1$  and  $V_2$ . Two photocurrent integrators,  $\Sigma_1$  and  $\Sigma_2$ , are used for the demodulation. The target distance,  $L_o$ , is given by

$$L_o = \frac{cT_p}{2} \left( 1 - \frac{V_1}{V_1 + V_2} \right), \quad (20)$$

where  $c$  is the light velocity and  $T_p$  is the pulse width. On the basis of Eq. (20), the output voltages of  $V_1$  and  $V_2$  are expected as shown Fig. 17(c).

Figure 18 shows measurement results of TOF range finding. The measurement setup employs a 5 MHz pulsed laser beam for spot projection since field projection requires a high flashlight intensity and a high photo sensitivity. The



**Fig. 18** Measured range accuracy of time-of-flight range finding.

laser beam source has 10 mW power and 665 nm wavelength. In the preliminary test, the present image sensor was operated at 40 MHz, and the TOF range finding was performed with no ambient light. The measured target range is between 600 mm and 1200 mm from the sensor. The range offset is calibrated at 900 mm, which mainly results from the delay of pulsed modulation. The error in the measured range is within  $\pm 150$  mm. The standard deviation of error is 73 mm. The large variations of the range are caused by demodulation signal jitter in high-speed demodulation and the low effective resolution of the on-chip AD conversion. The use of a high-resolution AD converter and uniformly distributed demodulation signals enable a high range resolution of TOF range finding. The preliminary test shows the feasibility of TOF range finding using the present image sensor.

## 7. Conclusions

A pixel-level color image sensor with efficient ambient light suppression has been presented. Bidirectional photocurrent integrators realize pixel-level demodulation of a modulated RGB flashlight with suppression of an ambient light at short intervals during an exposure period. Therefore, it avoids saturation from ambient illumination and realizes applicability of the color imaging under nonideal illumination conditions. Every pixel provides color information without false color or intensity loss of color filters. We have demonstrated the efficient ambient light suppression and the pixel-level color imaging using a  $64 \times 64$  prototype sensor. Moreover, TOF range finding with  $\pm 150$  mm range accuracy has been performed to show the feasibility of depth-key object extraction. The measurement results show that the present sensing scheme and circuit implementation realize a support capability of innate color capture and object extraction for image recognition in various measurement situations.

## Acknowledgment

The VLSI chip in this study has been fabricated through VLSI Design and Education Center (VDEC), the Univer-

sity of Tokyo, in collaboration with Rohm Corporation and Toppan Printing Corporation.

## References

- [1] Y. Ni and X.L. Yan, "CMOS active differential imaging device with single in-pixel analog memory," Proc. European Solid-State Circuits Conf. (ESSCIRC), pp.359–362, Sept. 2002.
- [2] M. Kawakita, T. Kurita, H. Hiroshi, and S. Inoue, "HDTV axi-vision camera," Proc. International Broadcasting Convention (IBC), pp.397–404, Sept. 2002.
- [3] A. Kimachi and S. Ando, "Time-domain correlation image sensor: First CMOS realization and evaluation," IEEE Int. Conf. Solid-State Sensors and Actuators, pp.958–961, June 1999.
- [4] J. Ohta, K. Yamamoto, T. Hirai, K. Kagawa, M. Nunoshita, M. Yamada, Y. Yamasaki, S. Sugishita, and K. Watanabe, "An image sensor with an in-pixel demodulation function for detecting the intensity of a modulated light signal," IEEE Trans. Electron Devices, vol.50, no.1, pp.166–172, Jan. 2003.
- [5] Y. Oike, M. Ikeda, and K. Asada, "High-sensitivity and wide-dynamic-range position sensor using logarithmic-response and correlation circuit," IEICE Trans. Electron., vol.E85-C, no.8, pp.1651–1658, Aug. 2002.
- [6] Y. Oike, M. Ikeda, and K. Asada, "A  $120 \times 110$  position sensor with the capability of sensitive and selective light detection in wide dynamic range for robust range finding," IEEE J. Solid-State Circuits, vol.39, no.1, pp.246–251, Jan. 2004.
- [7] Y. Oike, M. Ikeda, and K. Asada, "A pixel-level color image sensor with efficient ambient light suppression using modulated RGB flashlight and application to TOF range finding," IEEE Symp. VLSI Circuits Dig. of Tech. Papers, pp.298–301, June 2004.
- [8] R. Miyagawa and T. Kanade, "CCD-based range-finding sensor," IEEE Trans. Electron Devices, vol.44, no.10, pp.1648–1652, Oct. 1997.
- [9] S. Kawahito and I.A. Halin, "A time-of-flight range image sensor using inverting amplifiers," ITE Tech. Report, vol.27, no.59, pp.13–15, Oct. 2003.



**Yusuke Oike** received the B.S. and M.S. degrees in electronic engineering from the University of Tokyo, Tokyo, in 2000 and 2002, respectively. He is currently pursuing the Ph.D. degree at the Department of Electronic Engineering, the University of Tokyo. His current research interests include architecture and design of smart image sensors, mixed-signal circuits, and functional memories. He received Best Design Awards from IEEE International Conference on VLSI Design and IEEE/ACM

ASP-DAC in 2002 and 2004, respectively. He is a student member of the Institute of Electrical and Electronics Engineers (IEEE), and the Institute of Image Information and Television Engineers of Japan (ITEJ).



**Makoto Ikeda** received the B.S., M.S., and Ph.D. degrees in electronics engineering from the University of Tokyo, Tokyo, Japan, in 1991, 1993, and 1996, respectively. He joined the Department of Electronic Engineering, the University of Tokyo as a Faculty Member in 1996, and is currently an Associate Professor at VLSI Design and Education Center, the University of Tokyo. His research interests include the reliability of VLSI design. He is a member of the Institute of Electrical and Electronics Engineers (IEEE), and the Information Processing Society of Japan (IPJS).



**Kunihiro Asada** received the B.S., M.S., and Ph.D. degrees in electronic engineering from the University of Tokyo in 1975, 1977, and 1980, respectively. In 1980, he joined the Faculty of Engineering, the University of Tokyo, and became a lecturer, an associate professor and a professor in 1981, 1985 and 1995, respectively. From 1985 to 1986 he stayed in Edinburgh University as a visiting scholar supported by the British Council. From 1990 to 1992 he served as the first editor of the English version of IEICE (Institute of Electronics, Information and Communication Engineers of Japan) Transactions on Electronics. In 1996, he established VDEC (VLSI Design and Education Center) with his colleagues in the University of Tokyo. It is a government-supported center for promoting education and research of VLSI design in all the universities and colleges in Japan. He is currently the head of VDEC. His research interests are the design and evaluation of integrated systems and component devices. He has published more than 400 technical papers in journals and conference proceedings. He has received Best Paper Awards from IEEJ (Institute of Electrical Engineers of Japan), IEICE and ICMTS1998/IEEE, among others. He is a member of the Institute of Electrical and Electronics Engineers (IEEE), and the Institute of Electrical Engineers of Japan (IEEJ).